Supplementary Information

Effects of pH and light exposure on the survival of bacteria and their ability to biodegrade organic compounds in clouds: Implications for microbial activity in acidic cloud water

Yushuo Liu,[1,2] Chee Kent Lim,[1] Zhiyong Shen,[1] Patrick K. H. Lee,[1,3] Theodora Nah[1,2,3*]

[1]*School of Energy and Environment, City University of Hong Kong, Hong Kong SAR, China*
[2]*Shenzhen Research Institute, Nanshan District, Shenzhen, China*
[3]*State Key Laboratory of Marine Pollution, City University of Hong Kong, Hong Kong SAR, China*

** To whom correspondence should be addressed: Theodora Nah (Email: theodora.nah@cityu.edu.hk, Tel: +852 3442 5578)*

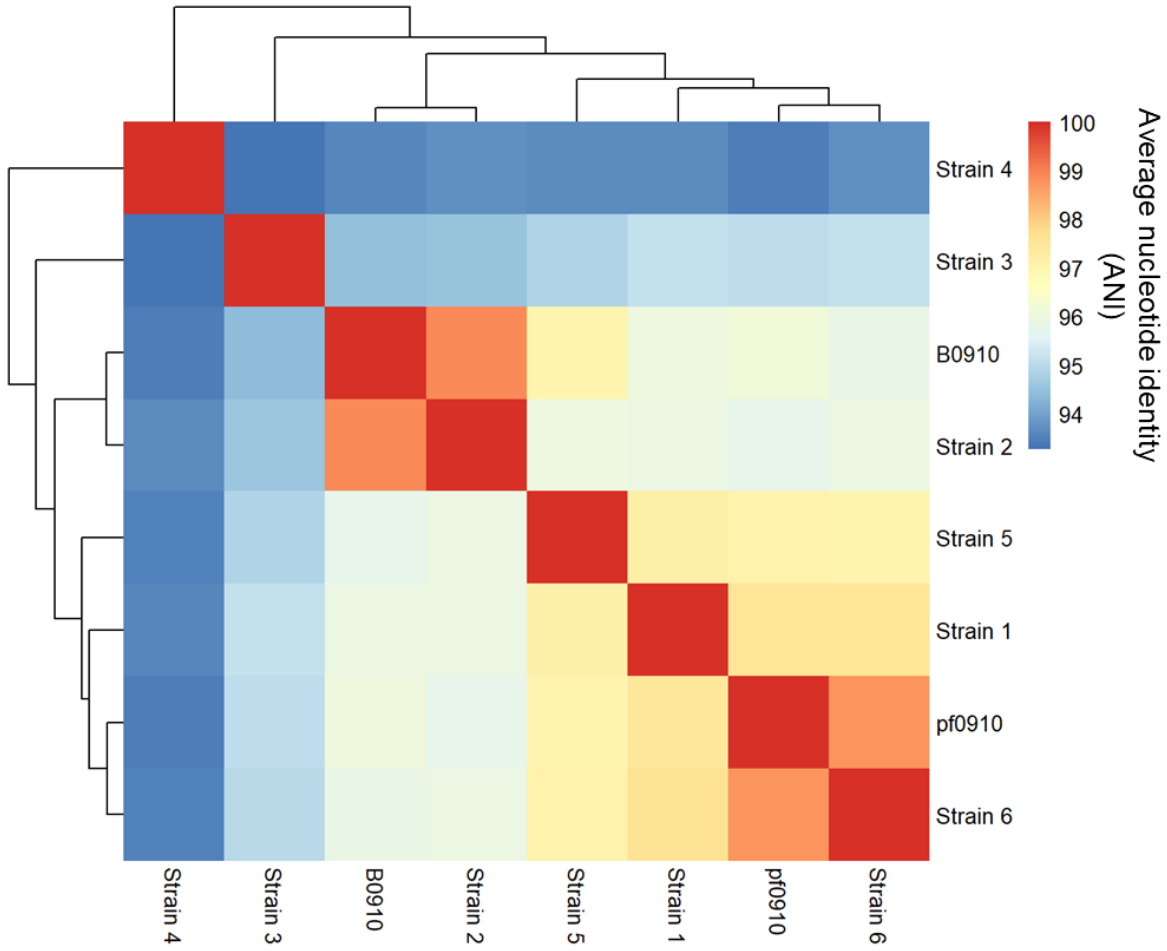

Figure S1. Average nucleotide identity (ANI) value of *Enterobacter* strains B00910, pf0910, and six others. **Strain 1:** *Enterobacter hormaechei* subsp. *oharae* DSM 16687; **Strain 2:** *Enterobacter hormaechei* subsp.hoffmannii DSM 14563; **Strain 3:** *Enterobacter hormaechei* ATCC 49162; **Strain 4**: *Enterobacter quasihormaechei*. GCF 004331385.1; **Strain 5:** *Enterobacter xiangfangensis* LMG27195; **Strain 6:** *Enterobacter hormaechei* subsp. *steigerwaltii* DSM 16691. Strains 1 to 6 are the closest identified neighbors with strains B0910 and pf0910.

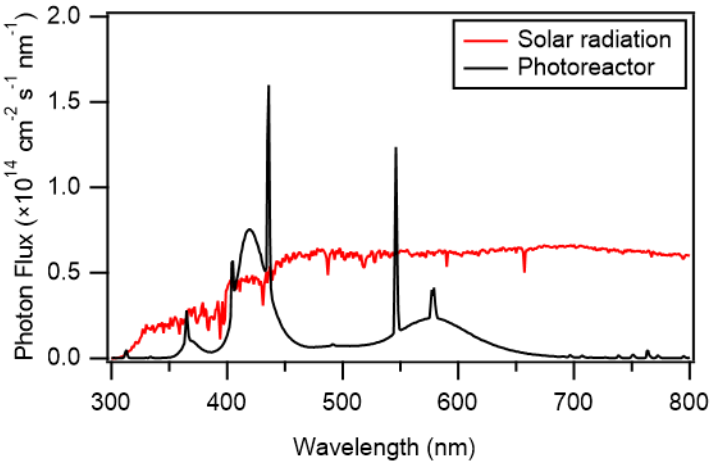

Figure S2. Photon flux inside of the photoreactor (black) and actinic flux for a fall day in Hong Kong in the morning (red). One lamp with output centered at ~365 nm (RPR-3500A, Southern New England Ultraviolet Company), four lamps with outputs centered at ~421 nm (RPR-4190A, Southern New England Ultraviolet Company), and three lamps with outputs centered at ~580 nm (RPR-5750A, Southern New England Ultraviolet Company) were used to illuminate solutions in the photoreactor.

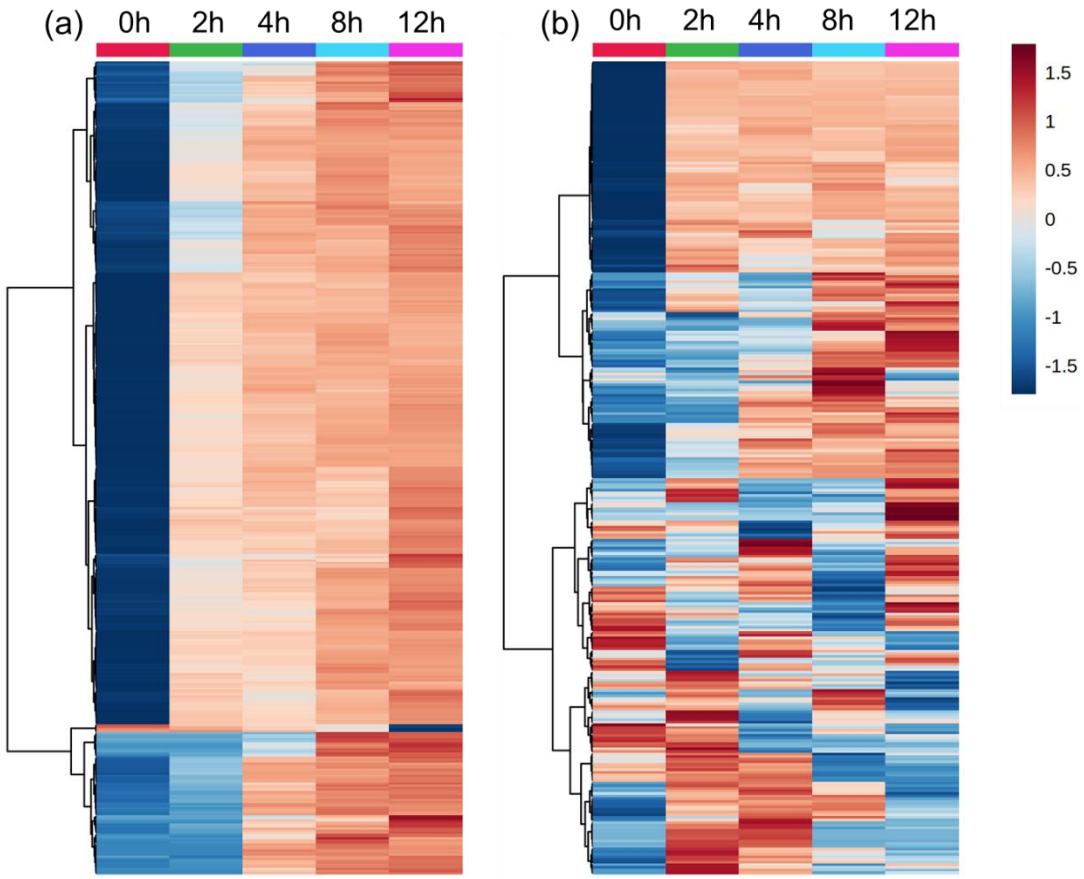

Figure S3. Heat maps showing the time evolution of (a) water-soluble compounds and (b) water-insoluble compounds from *E. hormaechei* B0910 during exposure to simulated sunlight at pH 4.3. The heat maps were generated from non-targeted UPLC-MS analysis of samples with different light exposure times. 259 water-soluble compounds and 215 water-insoluble compounds were selected based on PLS-DA results (VIP > 1.0 criteria). The average UPLC-MS intensity of each compound at each light exposure time was obtained from the nine replicates. The average UPLC-MS intensities were subsequently log10 transformed and auto scaled (i.e., mean-centered and divided by the standard deviation of each variable). The color scale ranges from red color for high abundance to blue for low abundance.

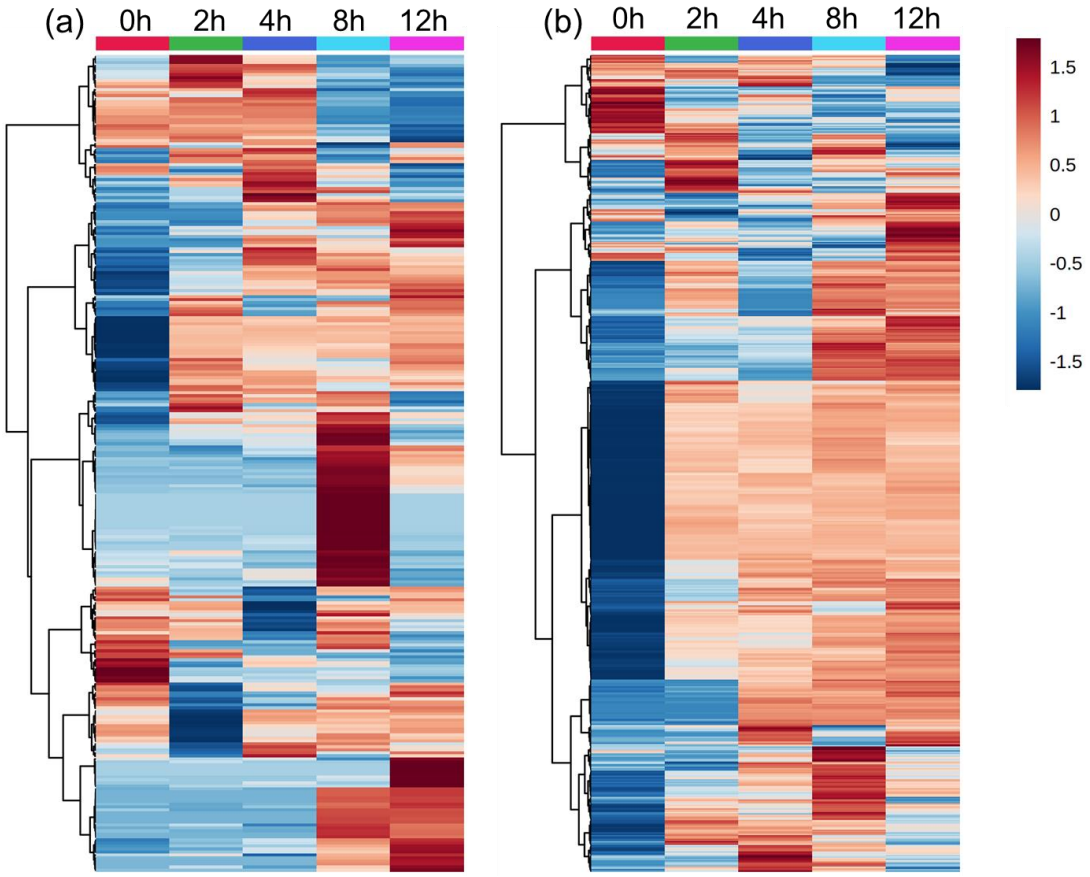

Figure S4. Heat maps showing the time evolution of (a) water-soluble compounds and (b) water-insoluble compounds from *E. hormaechei* pf0910 during exposure to simulated sunlight at pH 4.3. The heat maps were generated from non-targeted UPLC-MS analysis of samples with different light exposure times. 209 water-soluble compounds and 251 water-insoluble compounds were selected based on PLS-DA results (VIP > 1.0 criteria). The average UPLC-MS intensity of each compound at each light exposure time was obtained from the nine replicates. The average UPLC-MS intensities were subsequently log10 transformed and auto scaled (i.e., mean-centered and divided by the standard deviation of each variable). The color scale ranges from red color for high abundance to blue for low abundance.

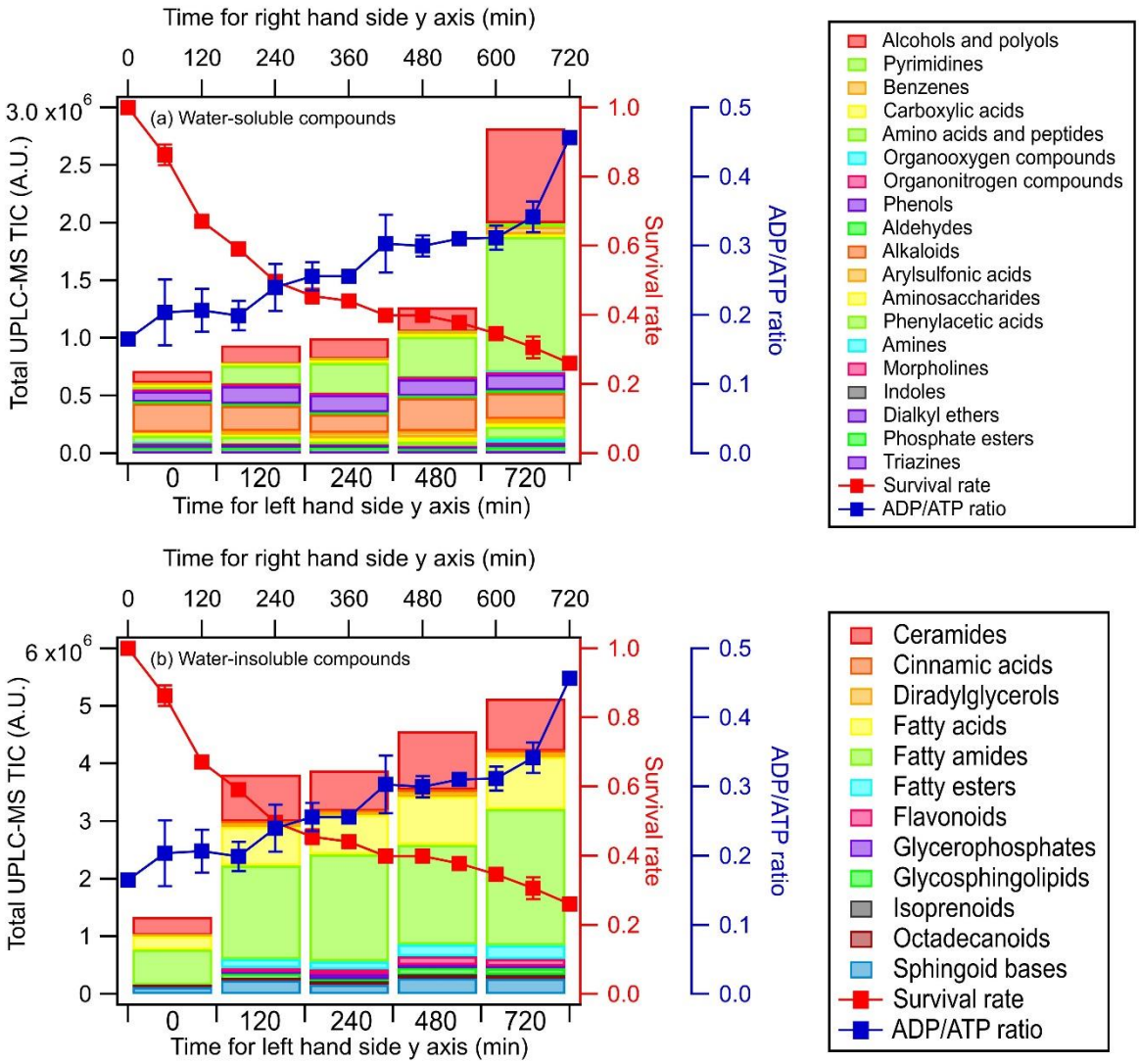

Figure S5. Time evolution of the UPLC-MS total ion chromatograph (TIC) signals of (a) water-soluble compounds, and (b) water-insoluble compounds from *E. hormaechei* pf0910 during exposure to simulated sunlight at pH 4.3 over time. These compounds are classified based on their chemical functionality. Also shown are the time evolution of the survival rate and ADP/ATP ratio of *E. hormaechei* pf0910.

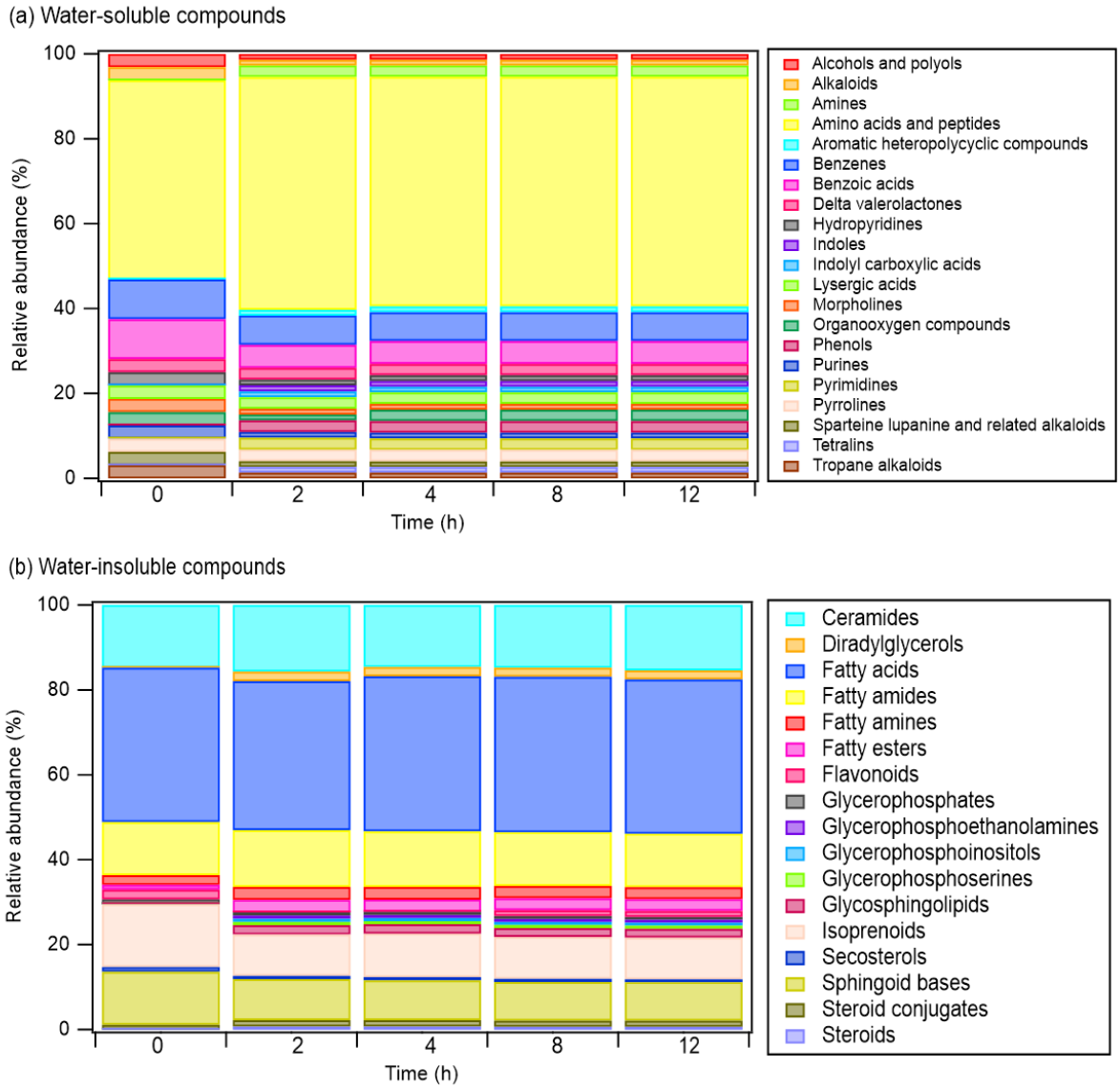

Figure S6. Relative abundance of the different classes of (a) water-soluble compounds, and (b) water-insoluble compounds from *E. hormaechei* B0910 during exposure to simulated sunlight at pH 4.3.

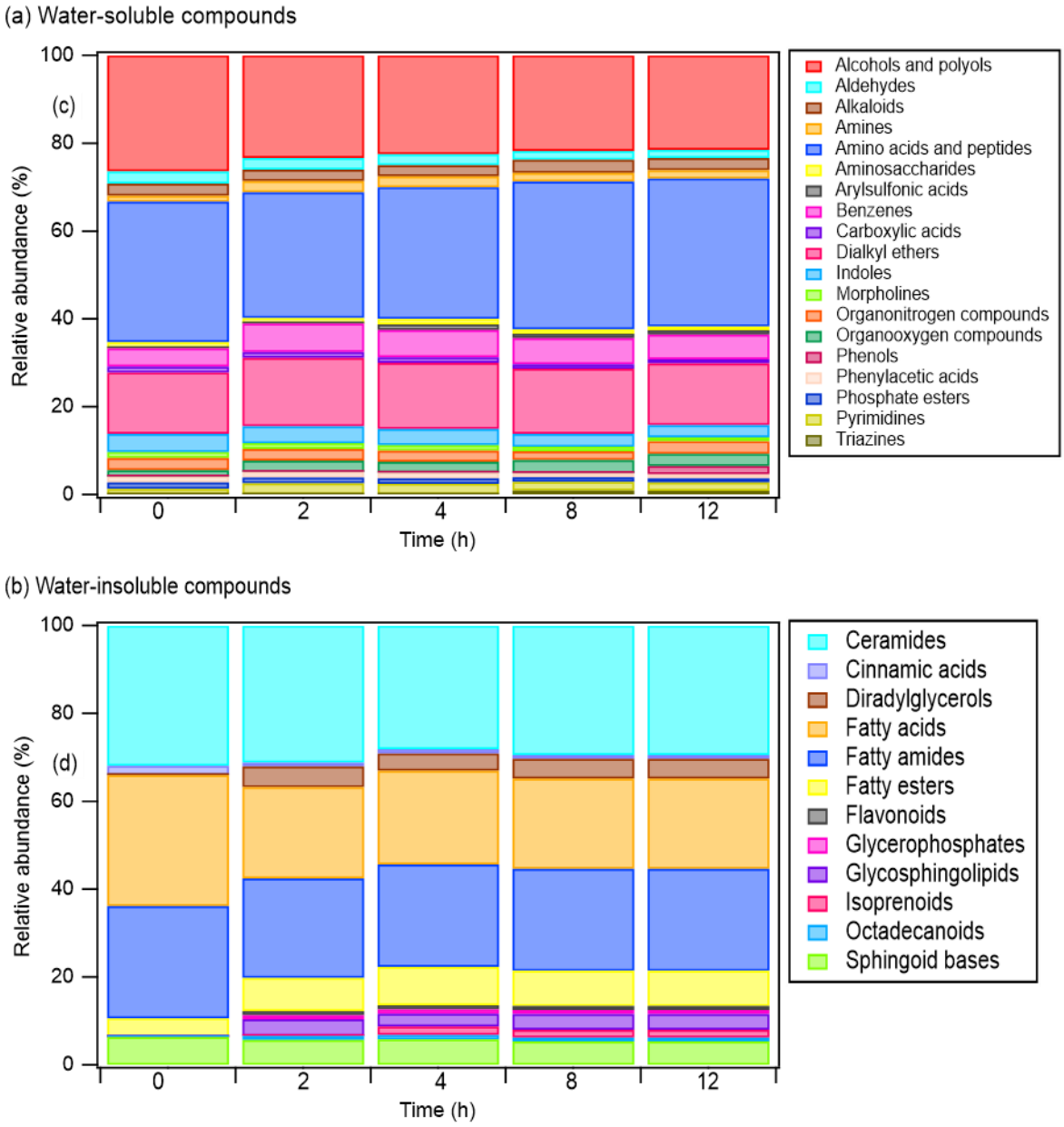

Figure S7. Relative abundance of the different classes of (c) water-soluble compounds, and (d) water-insoluble compounds from *E. hormaechei* pf0910 during exposure to simulated sunlight at pH 4.3.

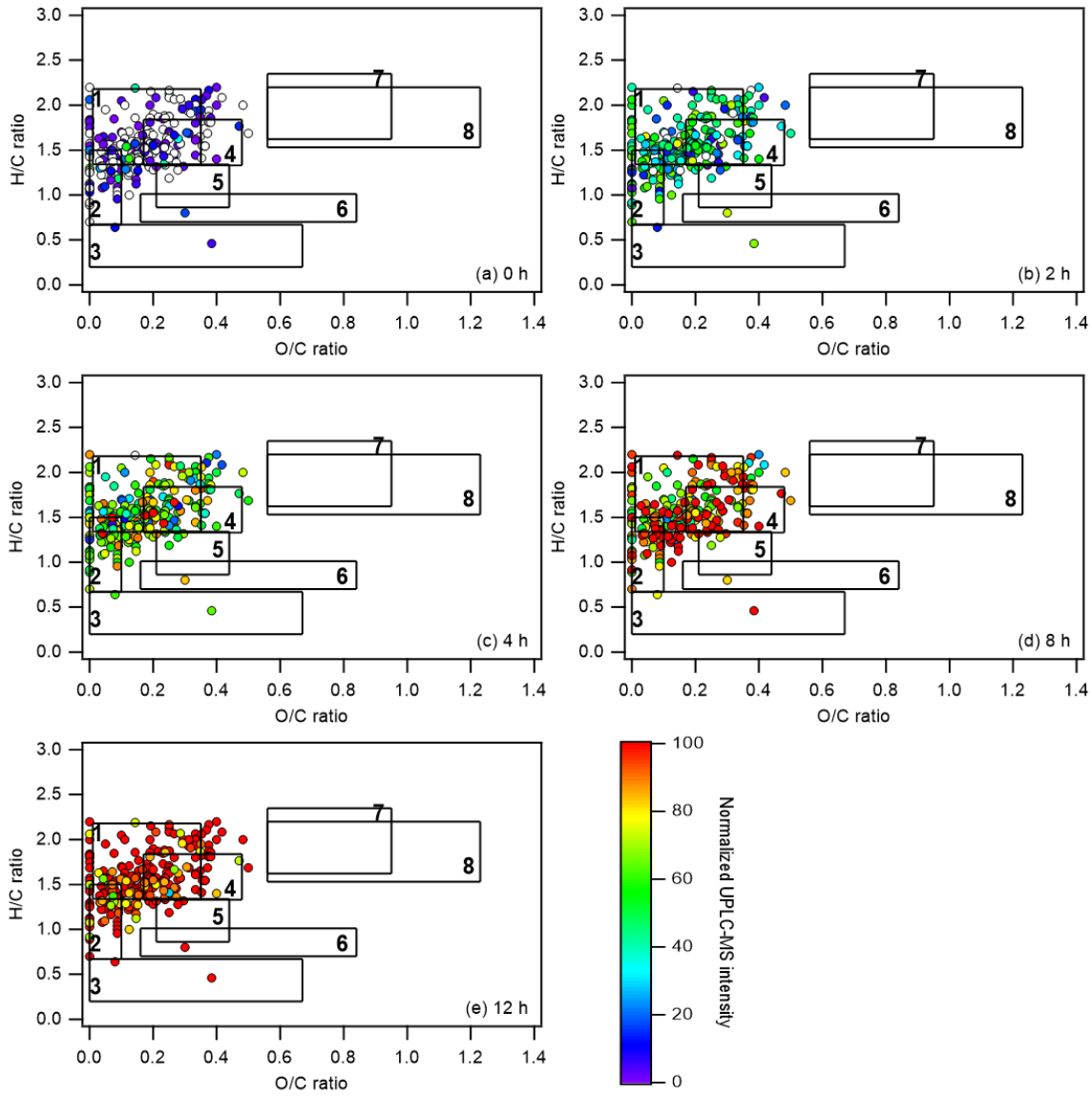

Figure S8. Van Krevelen diagrams of water-soluble compounds from *E. hormaechei* B0910 during exposure to simulated sunlight at pH 4.3 taken at different time points of the experiment: (a) 0 h, (b) 2 h, (c) 4 h, (d) 8 h, and (e) 12 h. The color of each symbol denotes its UPLC-MS intensity at that specific time point normalized to its maximum UPLC-MS intensity obtained during the entire experiment. Symbols that are colored white indicates that these compounds were not detected at that specific time point. The Van Krevelen diagrams are divided into eight chemical classes based on their O/C and H/C ratios: (1) lipids, (2) unsaturated hydrocarbons, (3) condensed aromatic structures, (4) peptides, (5) lignin, (6) tannin, (7) amino sugars, and (8) carbohydrates.

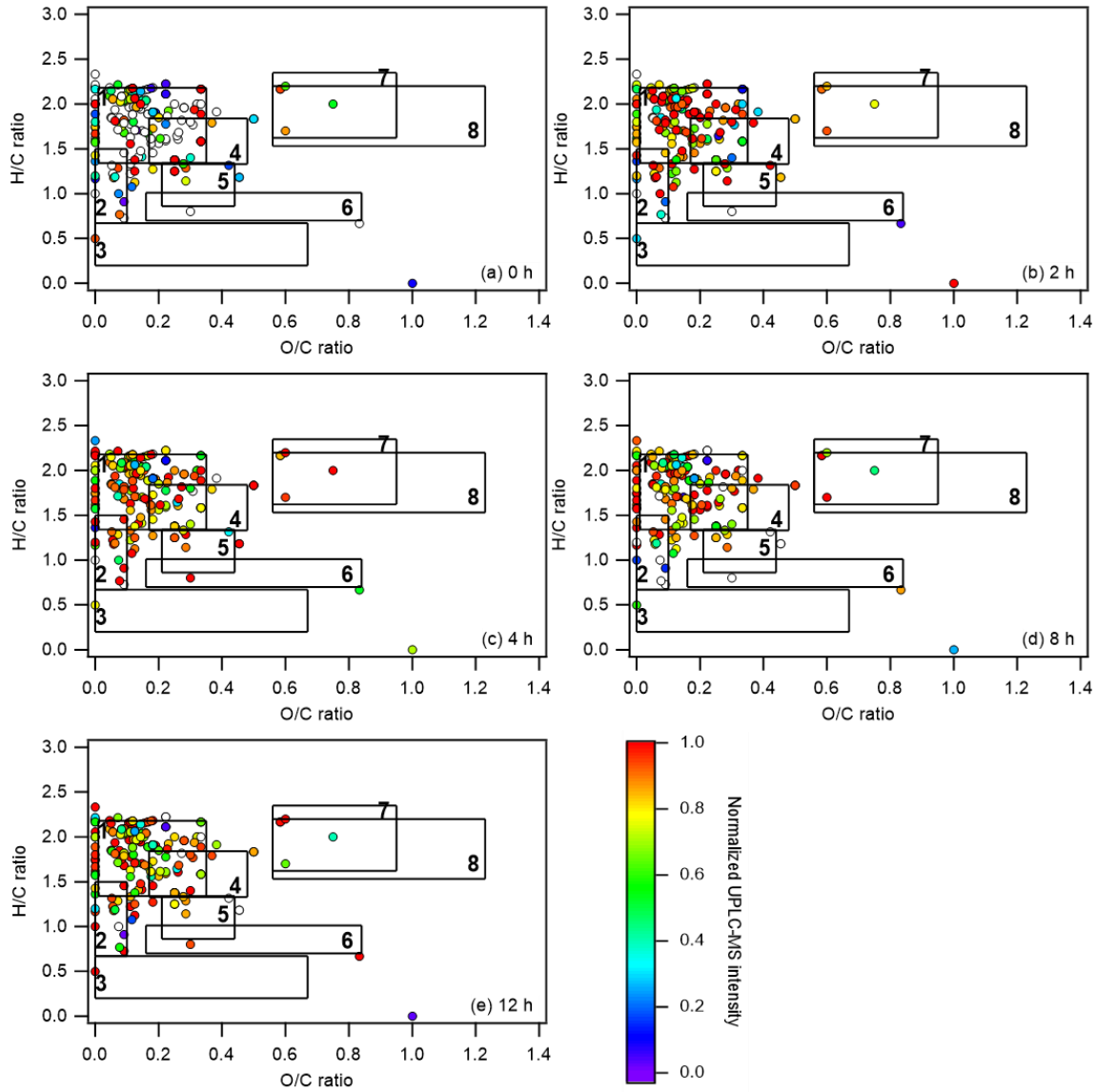

Figure S9. Van Krevelen diagrams of water-insoluble compounds from *E. hormaechei* B0910 during exposure to simulated sunlight at pH 4.3: (a) 0 h, (b) 2 h, (c) 4 h, (d) 8 h, and (e) 12 h. The color of each symbol denotes its UPLC-MS intensity at that specific time point normalized to its maximum UPLC-MS intensity obtained during the entire experiment. Symbols that are colored white indicates that these compounds were not detected at that specific time point. The Van Krevelen diagrams are divided into eight chemical classes based on their O/C and H/C ratios: (1) lipids, (2) unsaturated hydrocarbons, (3) condensed aromatic structures, (4) peptides, (5) lignin, (6) tannin, (7) amino sugars, and (8) carbohydrates.

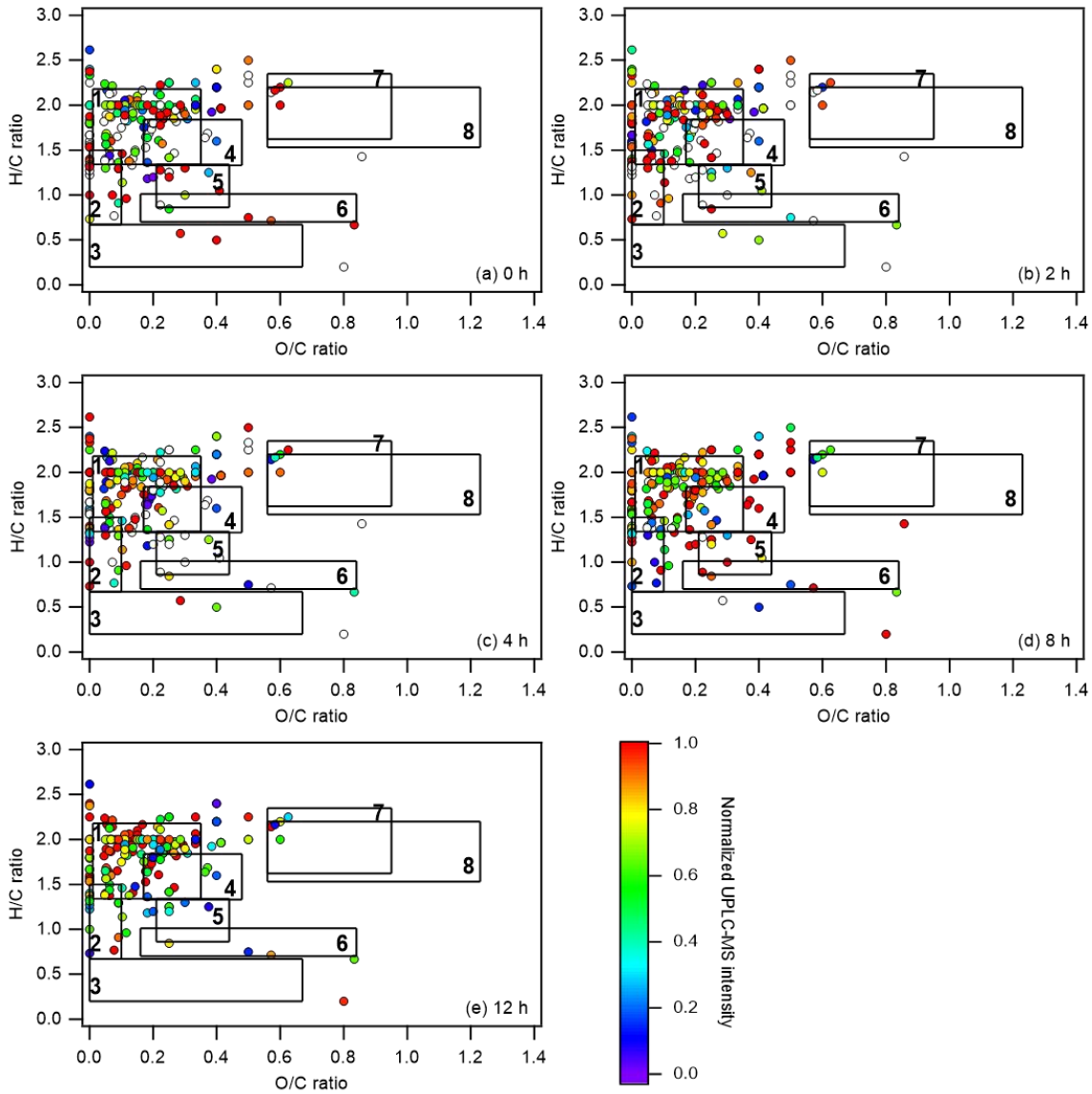

Figure S10. Van Krevelen diagrams of water-soluble compounds from *E. hormaechei* pf0910 during exposure to simulated sunlight at pH 4.3: (a) 0 h, (b) 2 h, (c) 4 h, (d) 8 h, and (e) 12 h. The color of each symbol denotes its UPLC-MS intensity at that specific time point normalized to its maximum UPLC-MS intensity obtained during the entire experiment. Symbols that are colored white indicates that these compounds were not detected at that specific time point. The Van Krevelen diagrams are divided into eight chemical classes based on their O/C and H/C ratios: (1) lipids, (2) unsaturated hydrocarbons, (3) condensed aromatic structures, (4) peptides, (5) lignin, (6) tannin, (7) amino sugars, and (8) carbohydrates.

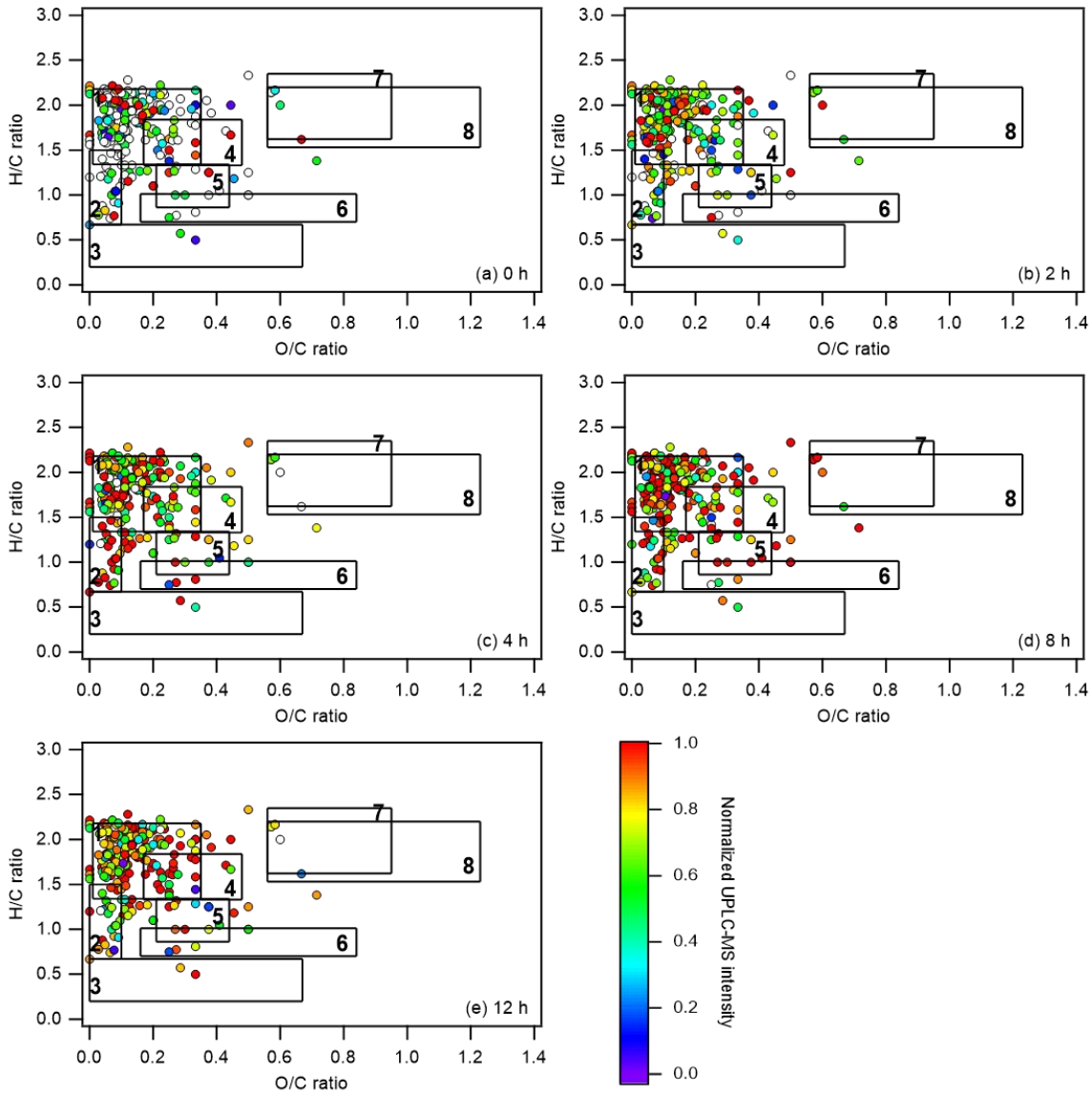

Figure S11. Van Krevelen diagrams of water-insoluble compounds from *E. hormaechei* pf0910 during exposure to simulated sunlight at pH 4.3: (a) 0 h, (b) 2 h, (c) 4 h, (d) 8 h, and (e) 12 h. The color of each symbol denotes its UPLC-MS intensity at that specific time point normalized to its maximum UPLC-MS intensity obtained during the entire experiment. Symbols that are colored white indicates that these compounds were not detected at that specific time point. The Van Krevelen diagrams are divided into eight chemical classes based on their O/C and H/C ratios: (1) lipids, (2) unsaturated hydrocarbons, (3) condensed aromatic structures, (4) peptides, (5) lignin, (6) tannin, (7) amino sugars, and (8) carbohydrates.

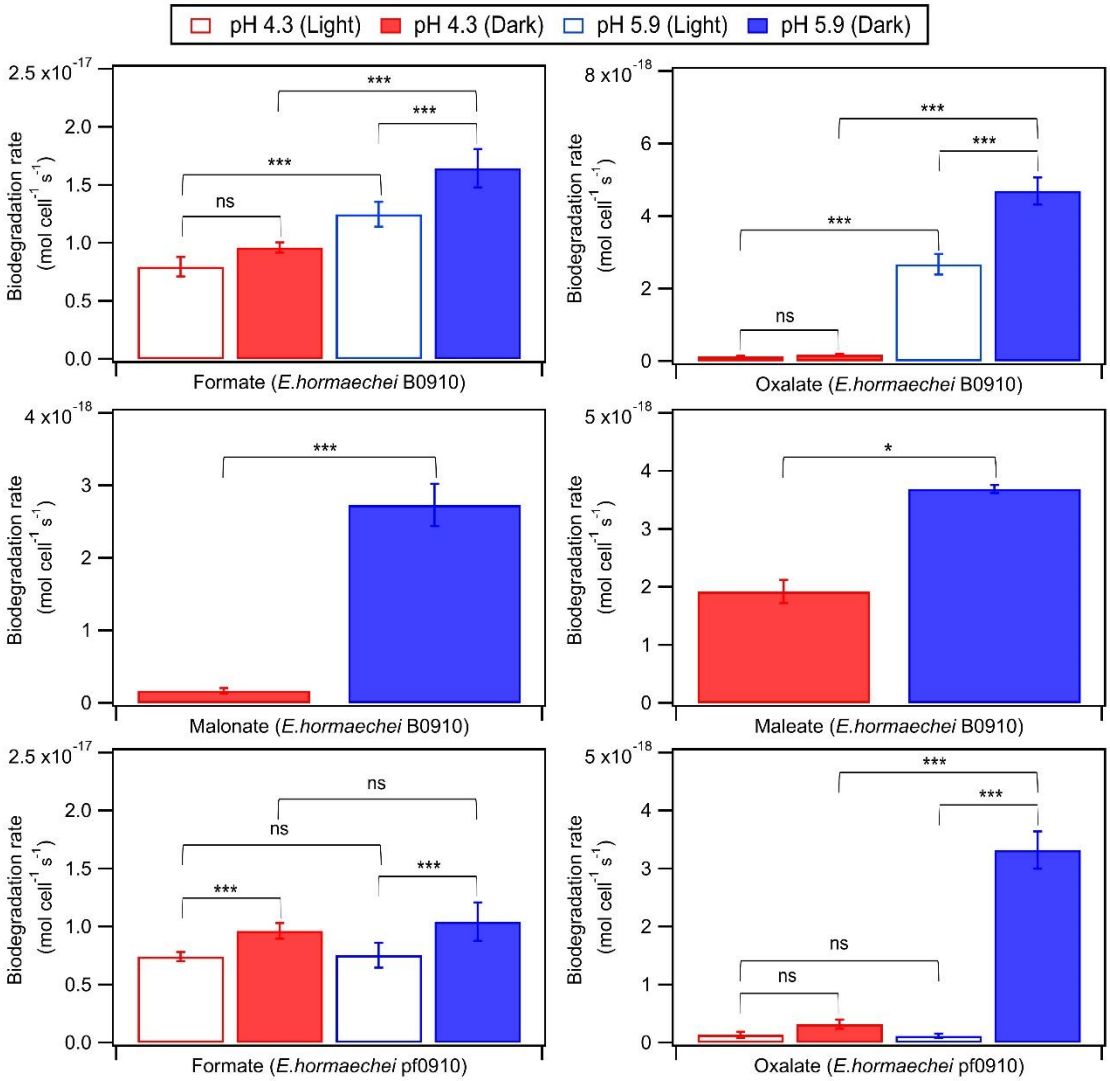

105

106 **Figure S12.** Biodegradation rates of oxalate, maleate, and malonate by (a) *E. hormaechei*
107 B0910 and (b) *E. hormaechei* pf0910 under light and dark conditions at pH 4.3 and pH 5.9.
108 Error bars represent one standard deviation from the mean of biological triplicates (ns: not
109 significant, *: *p* value < 0.05, **: *p* value < 0.01, ***: *p* value < 0.001).

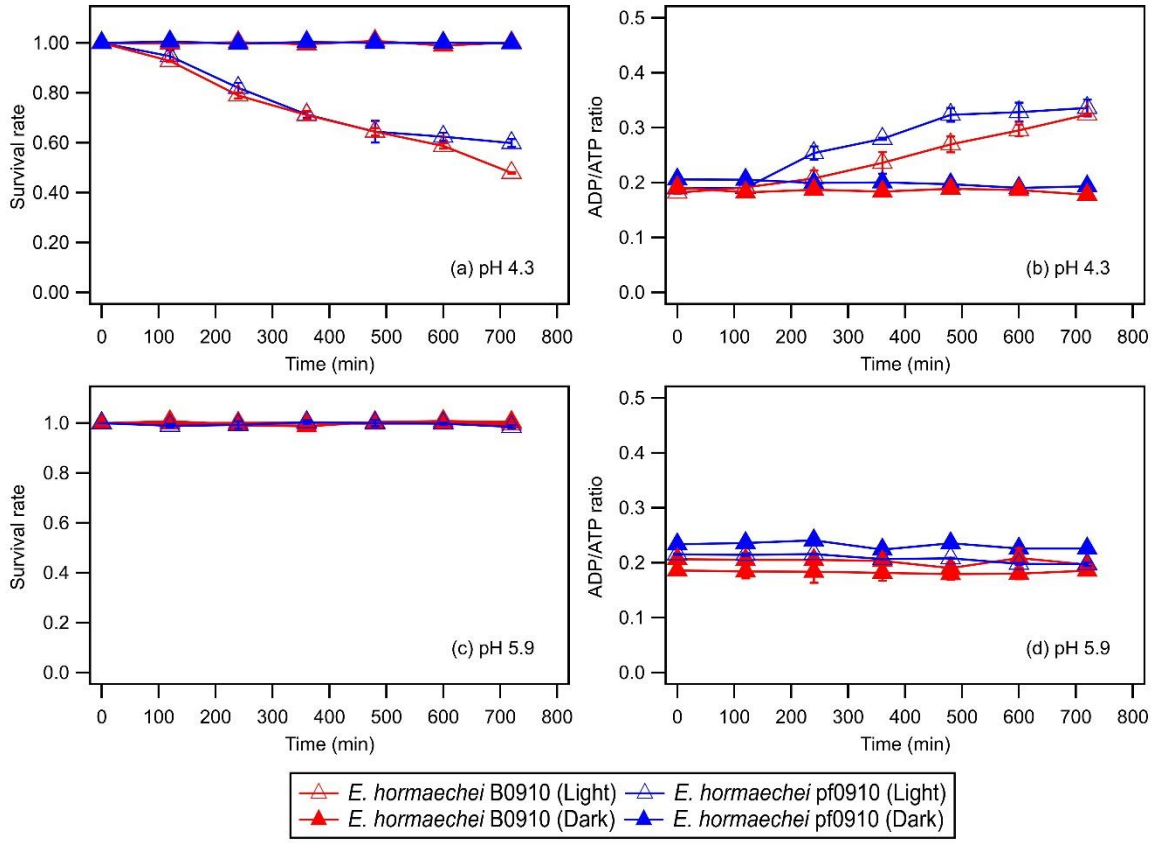

Figure S13. Survival and ADP/ATP ratios of *E. hormaechei* B0910 and *E. hormaechei* pf0910 under illuminated and dark conditions at pH 4.3 and pH 5.9 in the solutions containing the seven carboxylic acids. Error bars represent one standard deviation from the mean of biological triplicates.

Table S1. Chemical composition of the artificial cloud water used to prepare bacterial cells and perform experiments that investigated the effects of cloud water pH and light exposure on the survival and energetic metabolism of bacteria. In the experiments, the pH of the artificial cloud water was adjusted while keeping the final organic and inorganic ion composition the same.

Organic ion	μM	Inorganic ion	μM
Formate	17.1	Na^+	93
Acetate	10.2	NH_4^+	235
Pyruvate	2.7	K^+	8
Oxalate	10.3	Mg^{2+}	23
		Ca^{2+}	49
		Cl^-	138
		SO_4^{2-}	305

Table S2. Chemical composition of the artificial cloud water used for carboxylic acid biodegradation experiments.

Organic ion	μM	Inorganic ion	μM
Formate	50	Na^+	930
Acetate	50	NH_4^+	2350
Pyruvate	50	K^+	80
Oxalate	50	Mg^{2+}	230
Succinate	50	Ca^{2+}	490
Maleate	50	Cl^-	1380
Malonate	50	SO_4^{2-}	3050
Glutarate	50		
MSA	50		

142 **Table S3.** Stoichiometric ranges of the eight chemical classes in VK diagrams (Bianco et al.,
143 2018; Laszakovits and Mackay, 2022).

Chemical class	H/C	O/C
Amino sugar (Laszakovits and Mackay, 2022)	$1.62 \leq H/C \leq 2.35$	$0.56 \leq O/C \leq 0.95$
Carbohydrate (Laszakovits and Mackay, 2022)	$1.53 \leq H/C \leq 2.20$	$0.56 \leq O/C \leq 1.23$
Lignin (Laszakovits and Mackay, 2022)	$0.86 \leq H/C \leq 1.34$	$0.21 \leq O/C \leq 0.44$
Lipid (Laszakovits and Mackay, 2022)	$1.34 \leq H/C \leq 2.18$	$0.01 \leq O/C \leq 0.35$
Peptide (Laszakovits and Mackay, 2022)	$1.33 \leq H/C \leq 1.84$	$0.17 \leq O/C \leq 0.48$
Tannin (Laszakovits and Mackay, 2022)	$0.70 \leq H/C \leq 1.01$	$0.16 \leq O/C \leq 0.84$
Unsaturated hydrocarbons (Bianco et al., 2018)	$0.67 \leq H/C \leq 1.5$	$0 \leq O/C \leq 0.10$
Condensed aromatic structures (Bianco et al., 2018)	$0.20 \leq H/C \leq 0.67$	$0 \leq O/C \leq 0.67$

144

Table S4. Genes involved in the biodegradation of carboxylic acids in the two *E. hormaechei* strains.

Carboxylic acid	Genes	*E. hormaechei* B0910		*E. hormaechei* pf0910	
		Biodegradation	CDS	Biodegradation	CDS
		Yes/No	Absent/Present	Yes/No	Absent/Present
Formic acid	Formate dehydrogenase	Yes	AECJMNAI_01279; AECJMNAI_01280; AECJMNAI_01281; AECJMNAI_03442	Yes	CFAIMJNC_02488; CFAIMJNC_02489; CFAIMJNC_02490; CFAIMJNC_04681
Oxalic acid	Oxalate decarboxylase	Yes	Absent	Yes	Absent
	Oxalate oxidase	Yes	Absent	Yes	Absent
	Formyl-CoA:oxalate CoA-transferase	Yes	Absent	Yes	Absent
	Succinyl-CoA:oxalate CoA-transferase	Yes	Absent	Yes	Absent
	Hypothetical protein (Cupin 2 protein)[a]	Yes	AECJMNAI_00423	Yes	CFAIMJNC_01624
Malonic acid	Malonate decarboxylase	Yes	AECJMNAI_00917; AECJMNAI_00920; AECJMNAI_00921; AECJMNAI_00922; AECJMNAI_00924	No	CFAIMJNC_02108; CFAIMJNC_02111; CFAIMJNC_02112; CFAIMJNC_02113; CFAIMJNC_02115
	Malonate CoA-transferase	Yes	Absent	No	Absent
	Malonate-semialdehyde dehydrogenase	Yes	Absent	No	Absent
	Malonyl-CoA/methylmalonyl-CoA synthetase	Yes	Absent	No	Absent
Maleic acid	Maleate isomerase	Yes	Absent	No	Absent
	Maleate hydratase	Yes	Absent	No	Absent
	3-isopropylmalate dehydratase[a]	Yes	AECJMNAI_02091; AECJMNAI_02092	No	CFAIMJNC_03425; CFAIMJNC_03426
Acetic acid	Acetyl-CoA synthetase	No	AECJMNAI_01727	No	CFAIMJNC_02972
	Acetate kinase	No	AECJMNAI_04676	No	CFAIMJNC_00936
	Aldehyde dehydrogenase	No	AECJMNAI_01165	No	CFAIMJNC_02371

	ActP[b]	No	AECJMNAI_01725	No	CFAIMJNC_02970
	SatP[b]	No	AECJMNAI_02044	No	CFAIMJNC_03365
Methane sulfonic acid	Alkanesulfonate monooxygenase	No	AECJMNAI_03015; AECJMNAI_03017	No	CFAIMJNC_04351; CFAIMJNC_04353
Glutaric acid	Succinate-semialdehyde dehydrogenase / glutarate-semialdehyde dehydrogenase[c]	No	AECJMNAI_00812; AECJMNAI_01960	No	CFAIMJNC_02004; CFAIMJNC_03281
	Glutaryl-CoA synthetase	No	Absent	No	Absent
	Glutarate dioxygenase	No	Absent	No	Absent

[a] Genes are not canonical but may involve in the biodegradation of carboxylic acids.

[b] Transporter proteins involved in uptake of acetic acid for biodegradation

[c] No reverse catalysis in the direction from glutarate to glutarate-semialdehyde has been reported in the literature.

Table S5. Concentration of radicals and cells used to estimate the loss rates by biodegradation and chemical reactions in Table S6.

Radical concentration/ Cell concentration	Area	Concentration	Reference
·OH (M)	Remote	2.2×10^{-14}	(Herrmann et al., 2010)
	Marine	2.0×10^{-12}	(Herrmann et al., 2010)
	Urban	3.5×10^{-15}	(Herrmann et al., 2010)
NO_3· (M)	Remote	5.1×10^{-15}	(Herrmann et al., 2010)
	Marine	6.9×10^{-15}	(Herrmann et al., 2010)
	Urban	1.4×10^{-13}	(Herrmann et al., 2010)
Cell (cell L^{-1})		8.0×10^{7}	(Amato et al., 2007)

Table S6. Estimations of the loss rates of formate, oxalate, and malonate by biodegradation and chemical reactions (i.e., ·OH oxidation (daytime) and NO_3· (nighttime)). These loss rates were calculated based on concentrations and pH measured at the different sites. Equations used in these calculations can be found in Section S6. References used to obtain the pH of cloud/rainwater and carboxylic acids are indicated in superscripts. The biodegradation and chemical reaction loss rates calculated here were used to generate Figure 5.

Daytime

Location (remote)	Category	pH	Formate (μM)	Formate loss rate (M s^{-1})			Oxalate (μM)	Oxalate loss rate (M s^{-1})		
				bio (pH ~4)	bio (pH ~5)	·OH (remote)		bio (pH ~4)	bio (pH ~5)	·OH (remote)
Mount Lu(Sun et al., 2016)	Cloud	3.81 (Sun et al., 2016)	10.83 (Sun et al., 2016)	1.34×10^{-10}		5.72×10^{-10}	4.95 (Sun et al., 2016)	1.06×10^{-12}		1.74×10^{-11}
Mount Lu(Sun et al., 2016)	Rain	4.44 (Sun et al., 2016)	10.21 (Sun et al., 2016)	1.26×10^{-10}		5.39×10^{-10}	2.54 (Sun et al., 2016)	5.44×10^{-13}		8.92×10^{-12}
Mount Heng(Wang et al., 2011)	Cloud	3.8 (Wang et al., 2011)	19.65 (Wang et al., 2011)	2.43×10^{-10}		1.04×10^{-9}	5.11 (Wang et al., 2011)	1.10×10^{-12}		1.80×10^{-11}
Mount Heng(Wang et al., 2011)	Rain	4.35 (Wang et al., 2011)	14.30 (Wang et al., 2011)	1.77×10^{-10}		7.55×10^{-10}	1.66 (Wang et al., 2011)	3.55×10^{-13}		5.83×10^{-12}
Mangdang Mountain(Cheng et al., 2011)	Rain	4.81 (Cheng et al., 2011)	7.90 (Cheng et al., 2011)	9.78×10^{-11}		4.17×10^{-10}	1.80 (Cheng et al., 2011)	3.86×10^{-13}		6.34×10^{-12}
Taiwan(Tsai and Kuo, 2013)	Cloud	3.91 (Tsai and Kuo, 2013)	5.74 (Tsai and Kuo, 2013)	7.11×10^{-11}		3.03×10^{-10}	6.60 (Tsai and Kuo, 2013)	1.42×10^{-12}		2.32×10^{-11}
Kleiner Feldberg, Germany(Wobrock et al., 1994)	Cloud	3.9-4.6 (Wobrock et al., 1994)	3.26 (Wobrock et al., 1994)	4.03×10^{-11}		1.72×10^{-10}	ND			
Whiteface Mountain, USA(Khwaja et al., 1995)	Cloud	3.1-4.4 (Khwaja et al., 1995)	25.20 (Khwaja et al., 1995)	3.12×10^{-10}		1.33×10^{-9}	9.66 (Khwaja et al., 1995)	2.07×10^{-12}		3.40×10^{-11}
Rax, Austria(Löflund et al., 2002)	Cloud	3.84 (Löflund et al., 2002)	13.25 (Löflund et al., 2002)	1.64×10^{-10}		7.00×10^{-10}	5.11 (Löflund et al., 2002)	1.10×10^{-12}		1.80×10^{-11}
Sonnblick, Austria(Brantner et al., 1994)	Cloud	5.0-6.5 (Brantner et al., 1994)	6.30 (Brantner et al., 1994)		9.79×10^{-11}	3.33×10^{-10}	1.89 (Limbeck and Puxbaum, 2000)		3.61×10^{-12}	6.65×10^{-12}
Mount Tai, China(Guo et al., 2012)	Cloud	4.6 (Guo et al., 2012)	31.80 (Guo et al., 2012)	3.94×10^{-10}		1.68×10^{-9}	11.10 (Guo et al., 2012)	2.38×10^{-12}		3.91×10^{-11}
Shangzhong(Xu et al., 2009)	Rain	ND	4.95 (Xu et al., 2009)	6.13×10^{-11}		2.61×10^{-10}	1.16 (Xu et al., 2009)	2.48×10^{-13}		4.07×10^{-12}
São Paulo State, Brazil(Coelho et al., 2011)	Rain	4.96 (Coelho et al., 2011)	7.80 (Coelho et al., 2011)		1.21×10^{-10}	4.12×10^{-10}	1.20 (Coelho et al., 2011)		2.29×10^{-12}	4.22×10^{-12}

Location (Marine)	Category	pH	Formate (μM)	Formate loss rate (M s^{-1})			Oxalate (μM)	Oxalate loss rate (M s^{-1})		
				bio (pH ~4)	bio (pH ~5)	·OH (marine)		bio (pH ~4)	bio (pH ~5)	·OH (marine)
Puerto Rico	Cloud	5.5 (Gioda et al., 2011)	1.00 (Gioda et al., 2011)		1.55×10^{-11}	4.80×10^{-9}	0.50 (Gioda et al., 2011)		9.55×10^{-13}	1.60×10^{-10}
Puerto Rico(Gioda et al., 2011)	Rain	5.3 (Gioda et al., 2011)	0.20 (Gioda et al., 2011)		3.11×10^{-12}	9.60×10^{-10}	0.00 (Gioda et al., 2011)			

Puy de dome(Vaitilingom et al., 2013)	Cloud	6.1 (Vaitilingom et al., 2013)	4.90 (Vaitilingom et al., 2013)		7.61×10^{-11}	2.35×10^{-8}	1.00 (Vaitilingom et al., 2013)			1.91×10^{-12}	3.20×10^{-10}

Location (Urban)			Formate (μM)	Formate loss rate (M s^{-1})			Oxalate (μM)	Oxalate loss rate (M s^{-1})		
				bio (pH ~4)	bio (pH ~5)	·OH (urban)		bio (pH ~4)	bio (pH ~5)	·OH (urban)
Shenzhen, South China(Huang et al., 2010)	Rain	4.56 (Huang et al., 2010)	2.26 (Huang et al., 2010)	2.80×10^{-11}		1.90×10^{-11}	0.58 (Huang et al., 2010)	1.23×10^{-13}		3.22×10^{-13}
Anshun(Zhang et al., 2011)	Rain	4.67 (Zhang et al., 2011)	8.77 (Zhang et al., 2011)	1.09×10^{-10}		7.37×10^{-11}	2.84 (Zhang et al., 2011)	6.09×10^{-13}		1.59×10^{-12}
Newark US East Coast(Song and Gao, 2009)	Rain	4.6 (Song and Gao, 2009)	4.44 (Song and Gao, 2009)	5.50×10^{-11}		3.73×10^{-11}	0.68 (Song and Gao, 2009)	1.46×10^{-13}		3.81×10^{-13}
Hong Kong SAR(Li et al., 2020)	Cloud	3.87 (Li et al., 2020)	17.10 (Li et al., 2020)	2.12×10^{-10}		1.44×10^{-10}	10.30 (Li et al., 2020)	2.21×10^{-12}		5.77×10^{-12}
Puy de dome(Vaitilingom et al., 2013)	Cloud	3.9 (Vaitilingom et al., 2013)	33.20 (Vaitilingom et al., 2013)	4.11×10^{-10}		2.79×10^{-10}	9.30 (Vaitilingom et al., 2013)	1.99×10^{-12}		5.21×10^{-12}

ND: No data

Nighttime

Location (remote)	Category	pH	Formate (μM)	Formate loss rate (M s^{-1})			Oxalate (μM)	Oxalate loss rate (M s^{-1})			Malonate (μM)	Malonate loss rate (M s^{-1})		
				bio (pH ~4)	bio (pH ~5)	NO_3· (remote)		bio (pH ~4)	bio (pH ~5)	NO_3· (remote)		bio (pH ~4)	bio (pH ~5)	NO_3· (remote)
Mount Lu(Sun et al., 2016)	Cloud	3.81 (Sun et al., 2016)	10.83 (Sun et al., 2016)	1.69×10^{-10}		2.32×10^{-12}	4.95 (Sun et al., 2016)	2.07×10^{-12}		1.11×10^{-12}	ND			
Mount Lu(Sun et al., 2016)	Rain	4.44 (Sun et al., 2016)	10.21 (Sun et al., 2016)	1.59×10^{-10}		2.19×10^{-12}	2.54 (Sun et al., 2016)	1.06×10^{-12}		5.69×10^{-13}	ND			
Mount Heng(Wang et al., 2011)	Cloud	3.8 (Wang et al., 2011)	19.65 (Wang et al., 2011)	3.06×10^{-10}		4.21×10^{-12}	5.11 (Wang et al., 2011)	2.14×10^{-12}		1.15×10^{-12}	ND			
Mount Heng(Wang et al., 2011)	Rain	4.35 (Wang et al., 2011)	14.30 (Wang et al., 2011)	2.23×10^{-10}		3.06×10^{-12}	1.66 (Wang et al., 2011)	6.94×10^{-13}		3.71×10^{-13}	ND			
Mangdang Mountain(Cheng et al., 2011)	Rain	4.81 (Cheng et al., 2011)	7.90 (Cheng et al., 2011)	1.23×10^{-10}		1.69×10^{-12}	1.80 (Cheng et al., 2011)	7.55×10^{-13}		4.04×10^{-13}	1.40 (Cheng et al., 2011)		5.16×10^{-12}	4.00×10^{-14}
Taiwan(Tsai and Kuo, 2013)	Cloud	3.91 (Tsai and Kuo, 2013)	5.74 (Tsai and Kuo, 2013)	8.95×10^{-11}		1.23×10^{-12}	6.60 (Tsai and Kuo, 2013)	2.77×10^{-12}		1.48×10^{-12}	0.16 (Tsai and Kuo, 2013)	3.65×10^{-14}		4.57×10^{-15}
Kleiner Feldberg, Germany(Wobrock et al., 1994)	Cloud	3.9-4.6 (Wobrock et al., 1994)	3.26 (Wobrock et al., 1994)	5.08×10^{-11}		6.98×10^{-13}	ND				ND			
Whiteface Mountain, USA(Khwaja et al., 1995)	Cloud	3.1-4.4 (Khwaja et al., 1995)	25.20 (Khwaja et al., 1995)	3.93×10^{-10}		5.40×10^{-12}	9.66 (Khwaja et al., 1995)	4.05×10^{-12}		2.17×10^{-12}	7.69 (Khwaja et al., 1995)	1.75×10^{-12}		2.20×10^{-13}
Rax, Austria(Löflund et al., 2002)	Cloud	3.84 (Löflund et al., 2002)	13.25 (Löflund et al., 2002)	2.07×10^{-10}		2.84×10^{-12}	5.11 (Löflund et al., 2002)	2.14×10^{-12}		1.15×10^{-12}	1.92 (Löflund et al., 2002)	4.38×10^{-13}		5.49×10^{-14}
Sonnblick, Austria(Brantner et al., 1994)	Cloud	5.0-6.5 (Brantner et al., 1994)	6.30 (Brantner et al., 1994)		1.32×10^{-10}	1.35×10^{-12}	1.89 (Limbeck and Puxbaum, 2000)		1.19×10^{-11}	4.24×10^{-13}	0.38 (Limbeck and Puxbaum, 2000)		1.42×10^{-12}	1.10×10^{-14}
Mount Tai, China(Guo et al., 2012)	Cloud	4.6 (Guo et al., 2012)	31.80	4.96×10^{-10}		6.81×10^{-12}	11.10 (Guo et al., 2012)	4.65×10^{-12}		2.49×10^{-12}	ND			
Shangzhong(Xu et al.,	Rain		4.95	7.71×10^{-11}		1.06×10^{-12}	1.16	4.84×10^{-13}		2.59×10^{-13}	ND			

2009)														
São Paulo State, Brazil(Coelho et al., 2011)	Rain	4.96 (Coelho et al., 2011)	7.80 (Coelho et al., 2011)		1.63×10^{-10}	1.67×10^{-12}	1.20 (Coelho et al., 2011)		7.57×10^{-12}	2.69×10^{-13}	ND			

				Formate loss rate (M s^{-1})				Oxalate loss rate (M s^{-1})				Malonate loss rate (M s^{-1})		
Location (marine)		pH	Formate (μM)	bio (pH ~4)	bio (pH ~5)	$NO_3\cdot$ (marine)	Oxalate (μM)	bio (pH ~4)	bio (pH ~5)	$NO_3\cdot$ (marine)	Malonate (μM)	bio (pH ~4)	bio (pH ~5)	$NO_3\cdot$ (marine)
Puerto Rico(Gioda et al., 2011)	Cloud	5.5 (Gioda et al., 2011)	1.00 (Gioda et al., 2011)		2.09×10^{-11}	2.90×10^{-13}	0.50 (Gioda et al., 2011)		3.16×10^{-12}	1.52×10^{-13}	ND			
Puerto Rico(Gioda et al., 2011)	Rain	5.3 (Gioda et al., 2011)	0.20 (Gioda et al., 2011)		4.19×10^{-12}	5.80×10^{-14}	ND				ND			
Puy de dôme(Vaitilingom et al., 2013)	Cloud	6.1 (Vaitilingom et al., 2013)	4.90 (Vaitilingom et al., 2013)		1.03×10^{-10}	1.42×10^{-12}	1.00 (Vaitilingom et al., 2013)		6.31×10^{-12}	3.04×10^{-13}	0.40 (Vaïtilingom et al., 2012)		1.47×10^{-12}	1.55×10^{-14}

				Formate loss rate (M s^{-1})				Oxalate loss rate (M s^{-1})				Malonate loss rate (M s^{-1})		
Location (urban)		pH	Formate (μM)	bio (pH ~4)	bio (pH ~5)	$NO_3\cdot$ (urban)	Oxalate (μM)	bio (pH ~4)	bio (pH ~5)	$NO_3\cdot$ (urban)	Malonate (μM)	bio (pH ~4)	bio (pH ~5)	$NO_3\cdot$ (urban)
Shenzhen, South China(Huang et al., 2010)	Rain	4.56 (Huang et al., 2010)	2.26 (Huang et al., 2010)	3.52×10^{-11}		1.33×10^{-11}	0.58 (Huang et al., 2010)	2.41×10^{-13}		3.54×10^{-12}	ND			
Anshun(Zhang et al., 2011)	Rain	4.67 (Zhang et al., 2011)	8.77 (Zhang et al., 2011)	1.37×10^{-10}		5.16×10^{-11}	2.84 (Zhang et al., 2011)	1.19×10^{-12}		1.75×10^{-11}	ND			
Newark US East Coast(Song and Gao, 2009)	Rain	4.6 (Song and Gao, 2009)	4.44 (Song and Gao, 2009)	6.92×10^{-11}		2.61×10^{-11}	0.68 (Song and Gao, 2009)	2.85×10^{-13}		4.19×10^{-12}	0.29(Song and Gao, 2009)	6.61×10^{-14}		2.27×10^{-13}
Hong Kong SAR(Li et al., 2020)	Cloud	3.87 (Li et al., 2020)	17.10 (Li et al., 2020)	2.66×10^{-10}		1.01×10^{-10}	10.30 (Li et al., 2020)	4.32×10^{-12}		6.34×10^{-11}	1.36 (Zhao et al., 2019)	3.10×10^{-13}		1.07×10^{-12}
Puy de dome(Vaitilingom et al., 2013)	Cloud	3.9 (Vaitilingom et al., 2013)	33.20 (Vaitilingom et al., 2013)	5.17×10^{-10}		1.95×10^{-10}	9.30 (Vaitilingom et al., 2013)	3.90×10^{-12}		5.73×10^{-11}	3.50 (Vaitilingom et al., 2013)	7.97×10^{-13}		2.74×10^{-12}

ND: No data

Section S1. Genome assembly, annotation, and taxonomic analysis

Genome assembly of the sequencing reads was performed using the NECAT pipeline (v0.0.1_update20200803) (Chen et al., 2021) with the default parameters. The reads were first corrected (PREP_OUTPUT_COVERAGE = 40, CNS_OUTPUT_COVERAGE = 30, MIN_READ_LENGTH = 3000) and then the corrected reads were assembled (OVLP_FAST_OPTIONS = -n 500 -z 20 -b 2000 -e 0.5 -j 0 -u 1 -a 1000, OVLP_SENSITIVE_OPTIONS = -n 500 -z 10 -e 0.5 -j 0 -u 1 -a 1000). Both the correction and assembly steps were progressive with multiple processing steps to improve the accuracy and completeness. The quality of the assembled genomes was evaluated using the Benchmarking Universal Single-copy Orthologs (BUSCO v5.3.1) tool based on the database of enterobacterales_odb10 (Manni et al., 2021). For both strains B00910 and pf0910, complete circular chromosomes and plasmids were obtained.

Genome annotation was performed using Prokka (v1.14.6) (Seemann, 2014) with the default parameters. Whole genome-based taxonomic analysis was conducted using the Type (Strain) Genome Server (TYGS) (Meier-Kolthoff and Göker, 2019). Average Nucleotide Identity (ANI) was calculated by fastANI (v1.33) (Jain et al., 2018). Metabolic pathways were analyzed using the KEGG Mapper (Kanehisa et al., 2022) and the RAST server (Aziz et al., 2008). The sequences of the two genomes have been deposited in NCBI under the BioProject number PRJNA812965.

Section S2. Extraction of water-insoluble and water-soluble biological material and organic compounds for UPLC-MS analysis

A modified Bligh & Dyer (BD) protocol was performed to extract water-insoluble organic compounds (Sündermann et al., 2016). Briefly, 3 mL of methanol (Duskan, LC-MS grade)/chloroform (RCI, HPLC grade) (1:2, v/v) was added to a filtered 5 mL sample solution and vortexed for 5 min, after which the samples were centrifuged at 3000 rpm for 10 min at 10 ℃. The bottom layer was collected into a clean 2 mL centrifuge tube and dried in a concentrator using nitrogen gas. The dried extracts were redissolved in 500 µL of acetonitrile (Duskan, LC-MS grade) and stored at -20 ℃ prior to UPLC-MS analysis. Solid-phase extraction (SPE) was

performed to remove the inorganic salts and extract the water-soluble organic compounds using hydrophobic lipophilic balanced (HLB) cartridges (Oasis HLB, 6cc 500 mg). The HLB cartridges were first preconditioned with 1 mL methanol and 2 mL Milli-Q water. A 10 mL filtered sample solution was then loaded into the SPE cartridge and washed with 20 mL Milli-Q water under vacuum at a flow rate of 5 mL/min. The elution was performed by adding 1.5 mL methanol (Duskan, LC-MS grade). The eluent was evaporated to dryness under nitrogen gas and reconstituted in 500 µL acetonitrile (Duskan, LC-MS grade).

Section S3. UPLC-MS operation, data processing, and statistical analysis

Chromatographic separation was performed on a Kinetex HILIC LC column (100 × 2.1 mm, 2.6 µm, 100 Å, Phenomenex). The flow rate was fixed at 0.3 mL/min with ultra-pure water containing 5 mM ammonium acetate (Fisher, LC-MS grade) as mobile phase A and acetonitrile (Duskan, LC-MS grade) for mobile phase B. The following gradient program was used: 0 to 2 min 95% A; 2 to 4 min linear gradient to 80% B; 4 to 11 min linear gradient to 65% B; 11 to 12.5 min 65% B; 12.5 to 13 min linear gradient to 95% B; 13 to 15 min equilibration wash with 95% B. Injection volume was set at 10 uL. The information dependent analysis (IDA) acquisition was acquired with MS scan (100 to 1200 m/z) followed by MS/MS scan (50 to 1200 m/z) in positive ion mode. The following MS conditions were used: 30 PSI curtain gas, 60 PSI ion source gas, 3000 V ESI ion spray voltage, 320 ℃ source temperature, 10 V collision energy for MS, and 80 V declustering potential. MS/MS was acquired with a collision energy was 20 V with 5 V spread. The raw MS data was processed for peak detection, retention time correction, alignment, and integration using the XCMS software built into the web-based Galaxy platform (https://umsa.cerit-sc.cz/) (Gowda et al., 2014). The processed data was then uploaded to MetaboAnalyst 5.0 (https://www.metaboanalyst.ca/) (Pang et al., 2021) to identify cellular compounds that had prominent ion intensities.

The raw UPLC-MS data first underwent preprocessing, normalization, and quality control steps using the XCMS software built into the web-based Galaxy platform (available at: https://umsa.cerit-sc.cz/). The raw data was processed for peak detection, alignment, and framing. This generated a table that displayed the retention time, mass-to-charge ratio (m/z),

and the intensity/peak area for each peak. The quality control step was performed to assess the stability of the intensities of peaks ("features") between samples. This was performed using quality control samples, which were mixtures of equal amounts of experimental samples taken at each time point of the experiment. The relative standard deviation (RSD) of each feature in the quality control sample was compared to those in the experimental samples. Features with higher RSD in the quality control sample than in the experimental samples were excluded, while features with RSD < 30% were retained for further analysis. Multivariable statistical analysis was performed on the retained features using principal component analysis (PCA) with 95% confidence ellipse and partial least squares discrimination analysis (PLS-DA) to identify potential discriminations between the experimental samples. Heatmaps were generated to determine how the retained features changed at different time points during the experiment. A selection of discriminant ions and buckets was done based on the variable importance in projection (VIP) values. Features with VIP values greater than 1.0 were used for the identification step. MS/MS analysis was performed for the structural identification of compounds. The structure of each compound was deduced based on its adducts, isotopes, and MS/MS fragments using the SCIEX OS-Q software (AB Sciex). Information about compounds' chemical structures, m/z, and retention times were subsequently uploaded to MetaboAnalyst 5.0 (https://www.metaboanalyst.ca/), which used this information to identify the compounds.

Section S4. IC operation

Carboxylic acid concentrations were measured using a Dionex ICS-1100 (ThermoFisher Scientific) system. Separation was achieved using a Dionex IonPac AS18 (4 × 250 mm) anion exchange column (Thermo Scientific) equipped with a Dionex IonPac AG18 (4 × 50 mm) guard column (Thermo Scientific). 16 mM potassium hydroxide (Fisher, ≥85%) was used as the mobile phase at a flow rate of 1.0 mL/min for a 30 min run time. Each aliquot of solution was passed through a syringe filter before IC analysis.

Section S5. Possible enzymes and mechanisms associated with carboxylic acid biodegradation by the two bacterial strains

Table S4 summarized enzymes or metabolic pathways related to the biodegradation of carboxylic acids. Genes encoding formate dehydrogenases were identified in both genomes, which is consistent with the observed formate biodegradation. However, no known genes for oxalic acid biodegradation (Liu et al., 2021) were found in the genomes of both strains, which suggested the presence of yet to be characterized pathways that catalyzed the biodegradation. Interestingly, a protein with Cupin 2 domain was found in both genomes. The Cupin superfamily consists of a diverse range of enzymes including oxalate oxidase and oxalate decarboxylase that can biodegrade oxalic acid (Burrell et al., 2007).

Only the *E. hormaechei* B0910 strain was observed to biodegrade malonic acid. Interestingly, the malonyl-CoA-acyl carrier transcacylase observed in the *E. hormaechei* pf0910 strain seems to be a fusion protein, which may render it ineffective in utilizing malonic acid. Although no gene encoding maleate isomerase was identified in the genomes of both strains, the maleic acid biodegradation observed can be attributed to the activity of other enzymes with broad substrates specificity (Hatakeyama et al., 2000). The genes encoding for the small and large protein subunits that together form the 3-isopropylmalate dehydratase, the enzyme that isomerizes 2-isopropylmalate to 3-isopropylmalate, were found in both the *Enterobacter* strains. The small and large protein subunits of this enzyme are homologous to the small (51% amino acid identity) and large (59% amino acid identity) protein subunit constituents of maleate hydratase (HbzIJ) from *Pseudomonas alcaligenes* NCIMB 9867 that converts maleate to D-malate (Liu et al., 2015). Given the high protein homology, we speculate that the 3-isopropylmalate dehydratase in the *Enterobacter* strains may have a broader substrate specificity than known and it may be able to biodegrade maleate.

The lack of biodegradation of acetic acid, MSA, and glutaric acid in the experiments could be partly explained by the genomic information. Both strains have genes that encode enzymes involved in the biodegradation (Table S4) and associated uptake transporters (i.e., acetate permease (ActP) and succinate-acetate/proton symporter (SatP)) of acetic acid. The lack of the corresponding biodegradation in the experiments could be due to the low uptake of acetic acid by cells as ActP functions to scavenge low concentrations of the compound (Gimenez et al., 2003) while SatP could be inhibited by formic acid found in the cloud water

medium (Sá-Pessoa et al., 2013). Genes encoding the two-component alkanesulfonate monooxygenase for MSA biodegradation were found in both strains, but they were likely not expressed as sulfur was not deficient in the cloud water medium (Kahnert et al., 2000; Eichhorn and Leisinger, 2001), which is consistent with the absence of MSA biodegradation in the experiments. While genes encoding succinate-semialdehyde dehydrogenase/glutarate-semialdehyde dehydrogenase, which display a reversible conversion between glutarate-semialdehyde and glutarate in the KEGG database (Kanehisa et al., 2022), were found in both strains, to our knowledge there is no report of experimental results confirming that the reaction can go in the reverse direction from glutarate to glutarate-semialdehyde. In addition, a study of glutaric semialdehyde dehydrogenase reported the irreversible nature of the catalysis of glutarate semialdehyde to glutarate (Ichihara and Ichihara, 1961). Thus, it is not surprising that glutarate biodegradation was not observed for the two strains.

Section S6. Estimation of biodegradation and chemical reaction rates (M s^{-1}) in cloud water

S6.1. Biodegradation

The decay in the concentration of a specific carboxylic acid as a function of time during a biodegradation experiment can be described by the following equation:

$$\frac{d[Acid]}{dt} = k'_{cell} \times [Acid] = k_{cell,acid} \times [cell]_{experiment} \times [Acid]_{experiment}$$

where k'_{cell} (s^{-1}) is the pseudo first order rate constant obtained from fitting the decay of the carboxylic acid, and $[Acid]_{experiment}$ ($mol\ L^{-1}$) is the initial concentration of the carboxylic acid used in the biodegradation experiment. k'_{cell} is the product of the concentration of bacteria cells used in the experiment ($[cell]_{experiment}, cell\ L^{-1}$) and the biodegradation rate constant ($k_{cell,acid}$, $L\ cell^{-1}s^{-1}$).

The loss rate of the carboxylic acid in cloud water resulting from biodegradation is:

$$\frac{d[Acid]_{cloud}}{dt} = k_{cell,acid} \times [cell]_{cloud} \times [Acid]_{cloud}$$

where $[cell]_{cloud}$ ($cell\ L^{-1}$) is the concentration of bacteria cells present in cloud water ($cell\ L^{-1}$), and $[Acid]_{cloud}$ ($mol\ L^{-1}$) is the concentration of the carboxylic in cloud water.

S6.2. Chemical reactions

The loss rates of the carboxylic acid in cloud water resulting from reactions with ·OH and NO_3· are:

$$\frac{d[Acid]_{cloud}}{dt} = k_{OH,acid} \times [\cdot OH]_{cloud} \times [Acid]_{cloud}$$

$$\frac{d[Acid]_{cloud}}{dt} = k_{NO3,acid} \times [NO_3 \cdot]_{cloud} \times [Acid]_{cloud}$$

where $k_{OH,acid}$ ($L\ mol^{-1}s^{-1}$) and $k_{NO3,acid}$ ($L\ mol^{-1}s^{-1}$) are the rate constants for the reactions of the carboxylic acid with ·OH and NO_3·, respectively, and $[\cdot OH]_{cloud}$ ($mol\ L^{-1}$) and $[NO_3 \cdot]_{cloud}$ ($mol\ L^{-1}$) are the concentrations of ·OH and NO_3· in cloud water, respectively.

References

Amato, P., Parazols, M., Sancelme, M., Mailhot, G., Laj, P., and Delort, A.-M.: An important oceanic source of micro-organisms for cloud water at the Puy de Dôme (France), Atmospheric Environment, 41, 8253-8263, https://doi.org/10.1016/j.atmosenv.2007.06.022, 2007.

Aziz, R. K., Bartels, D., Best, A. A., DeJongh, M., Disz, T., Edwards, R. A., Formsma, K., Gerdes, S., Glass, E. M., and Kubal, M.: The RAST Server: rapid annotations using subsystems technology, BMC genomics, 9, 1-15, https://doi.org/10.1186/1471-2164-9-75, 2008.

Bianco, A., Deguillaume, L., Vaitilingom, M., Nicol, E., Baray, J. L., Chaumerliac, N., and Bridoux, M.: Molecular Characterization of Cloud Water Samples Collected at the Puy de Dome (France) by Fourier Transform Ion Cyclotron Resonance Mass Spectrometry, Environmental Science & Technology, 52, 10275-10285, https://doi.org/10.1021/acs.est.8b01964, 2018.

Brantner, B., Fierlinger, H., Puxbaum, H., and Berner, A.: Cloudwater chemistry in the subcooled droplet regime at Mount Sonnblick (3106 m asl, Salzburg, Austria), Water, Air, and Soil Pollution, 74, 363-384, https://doi.org/10.1007/BF00479800, 1994.

Burrell, M. R., Just, V. J., Bowater, L., Fairhurst, S. A., Requena, L., Lawson, D. M., and Bornemann, S.: Oxalate decarboxylase and oxalate oxidase activities can be interchanged with a specificity switch of up to 282 000 by mutating an active site lid, Biochemistry, 46, 12327-12336, https://doi.org/10.1021/bi700947s, 2007.

Chen, Y., Nie, F., Xie, S.-Q., Zheng, Y.-F., Dai, Q., Bray, T., Wang, Y.-X., Xing, J.-F., Huang, Z.-J., and Wang, D.-P.: Efficient assembly of nanopore reads via highly accurate and intact error correction, Nature Communications, 12, 1-10, https://doi.org/10.1038/s41467-020-20236-7, 2021.

Cheng, Y., Liu, Y., Huo, M., Sun, Q., Wang, H., Chen, Z., and Bai, Y.: Chemical characteristics of precipitation at Nanping Mangdang Mountain in eastern China during spring, Journal of Environmental Sciences, 23, 1350-1358, https://doi.org/10.1016/S1001-0742(10)60560-8, 2011.

Coelho, C. H., Allen, A. G., Fornaro, A., Orlando, E. A., Grigoletto, T. L., and Campos, M. L. A.: Wet deposition of major ions in a rural area impacted by biomass burning emissions, Atmospheric environment, 45, 5260-5265, https://doi.org/10.1016/j.atmosenv.2011.06.063, 2011.

Eichhorn, E. and Leisinger, T.: Escherichia coli utilizes methanesulfonate and L-cysteate as sole sulfur sources for growth, FEMS microbiology letters, 205, 271-275, https://doi.org/10.1111/j.1574-6968.2001.tb10960.x, 2001.

Gimenez, R., Nuñez, M. F., Badia, J., Aguilar, J., and Baldoma, L.: The gene yjcG, cotranscribed with the gene acs, encodes an acetate permease in Escherichia coli, Journal of bacteriology, 185, 6448-6455, https://doi.org/10.1128/JB.185.21.6448-6455.2003, 2003.

Gioda, A., Reyes-Rodriguez, G. J., Santos-Figueroa, G., Collett, J. L., Decesari, S., Ramos, M., Netto, H., Neto, F. R. D., and Mayol-Bracero, O. L.: Speciation of water-soluble inorganic, organic, and total nitrogen in a background marine environment: Cloud water, rainwater, and aerosol particles, Journal of Geophysical Research-Atmospheres, 116, https://doi.org/10.1029/2010jd015010, 2011.

Gowda, H., Ivanisevic, J., Johnson, C. H., Kurczy, M. E., Benton, H. P., Rinehart, D., Nguyen, T., Ray, J., Kuehl, J., Arevalo, B., Westenskow, P. D., Wang, J., Arkin, A. P., Deutschbauer, A. M., Patti, G. J., and Siuzdak, G.: Interactive XCMS Online: simplifying advanced metabolomic data processing and subsequent statistical analyses, Anal Chem, 86, 6931-6939, https://doi.org/10.1021/ac500734c, 2014.

Guo, J., Wang, Y., Shen, X., Wang, Z., Lee, T., Wang, X., Li, P., Sun, M., Collett Jr, J. L., and Wang, W.: Characterization of cloud water chemistry at Mount Tai, China: Seasonal variation, anthropogenic impact, and cloud processing, Atmospheric Environment, 60, 467-476, https://doi.org/10.1016/j.atmosenv.2012.07.016, 2012.

Hatakeyama, K., GoTo, M., Kobayashi, M., Terasawa, M., and Yukawa, H.: Analysis of oxidation sensitivity of maleate cis-trans isomerase from Serratia marcescens, Bioscience, biotechnology, and biochemistry, 64, 1477-1485, https://doi.org/10.1271/bbb.64.1477, 2000.

Herrmann, H., Hoffmann, D., Schaefer, T., Brauer, P., and Tilgner, A.: Tropospheric aqueous-phase free-radical chemistry: radical sources, spectra, reaction kinetics and prediction tools,

Chemphyschem, 11, 3796-3822, https://doi.org/10.1002/cphc.201000533, 2010.

Huang, X.-F., Li, X., He, L.-Y., Feng, N., Hu, M., Niu, Y.-W., and Zeng, L.-W.: 5-Year study of rainwater chemistry in a coastal mega-city in South China, Atmospheric Research, 97, 185-193, https://doi.org/10.1016/j.atmosres.2010.03.027, 2010.

Ichihara, A. and Ichihara, E. A.: Metabolism of L-Lysine by Bacterial Enzymes V. Glutaric Semialdehyde Dehydrogenase, The Journal of Biochemistry, 49, 154-157, https://doi.org/10.1093/oxfordjournals.jbchem.a127272, 1961.

Jain, C., Rodriguez-R, L. M., Phillippy, A. M., Konstantinidis, K. T., and Aluru, S.: High throughput ANI analysis of 90K prokaryotic genomes reveals clear species boundaries, Nature communications, 9, 1-8, https://doi.org/10.1038/s41467-018-07641-9, 2018.

Kahnert, A., Vermeij, P., Wietek, C., James, P., Leisinger, T., and Kertesz, M. A.: The ssu locus plays a key role in organosulfur metabolism in Pseudomonas putida S-313, Journal of bacteriology, 182, 2869-2878, https://doi.org/10.1128/JB.182.10.2869-2878.2000, 2000.

Kanehisa, M., Sato, Y., and Kawashima, M.: KEGG mapping tools for uncovering hidden features in biological data, Protein Science, 31, 47-53, https://doi.org/10.1002/pro.4172, 2022.

Khwaja, H. A., Brudnoy, S., and Husain, L.: Chemical characterization of three summer cloud episodes at Whiteface Mountain, Chemosphere, 31, 3357-3381, https://doi.org/10.1016/0045-6535(95)00187-D, 1995.

Laszakovits, J. R. and MacKay, A. A.: Data-Based Chemical Class Regions for Van Krevelen Diagrams, Journal of the American Society for Mass Spectrometry, 33, 198-202, https://doi.org/10.1021/jasms.1c00230, 2022.

Li, T., Wang, Z., Wang, Y., Wu, C., Liang, Y., Xia, M., Yu, C., Yun, H., Wang, W., Wang, Y., Guo, J., Herrmann, H., and Wang, T.: Chemical characteristics of cloud water and the impacts on aerosol properties at a subtropical mountain site in Hong Kong SAR, Atmospheric Chemistry and Physics, 20, 391-407, https://doi.org/10.5194/acp-20-391-2020, 2020.

Limbeck, A. and Puxbaum, H.: Dependence of in-cloud scavenging of polar organic aerosol compounds on the water solubility, Journal of Geophysical Research-Atmospheres, 105, 19857-19867, https://doi.org/10.1029/2000jd900123, 2000.

Liu, K., Xu, Y., and Zhou, N.-Y.: Identification of a specific maleate hydratase in the direct hydrolysis route of the gentisate pathway, Applied and Environmental Microbiology, 81, 5753-5760, https://doi.org/10.1128/AEM.00975-15, 2015.

Liu, M., Devlin, J. C., Hu, J., Volkova, A., Battaglia, T. W., Ho, M., Asplin, J. R., Byrd, A., Li, H., and Ruggles, K. V.: Microbial genetic and transcriptional contributions to oxalate degradation by the gut microbiota in health and disease, Elife, 10, e63642, https://doi.org/10.7554/eLife.63642, 2021.

Löflund, M., Kasper-Giebl, A., Schuster, B., Giebl, H., Hitzenberger, R., and Puxbaum, H.: Formic, acetic, oxalic, malonic and succinic acid concentrations and their contribution to organic carbon in cloud water, Atmospheric Environment, 36, 1553-1558, https://doi.org/10.1016/S1352-2310(01)00573-8, 2002.

Manni, M., Berkeley, M. R., Seppey, M., and Zdobnov, E. M.: BUSCO: assessing genomic data quality and beyond, Current Protocols, 1, e323, https://doi.org/10.1002/cpz1.323, 2021.

Meier-Kolthoff, J. P. and Göker, M.: TYGS is an automated high-throughput platform for state-of-the-art genome-based taxonomy, Nature communications, 10, 1-10, https://doi.org/10.1038/s41467-019-10210-3, 2019.

Pang, Z., Chong, J., Zhou, G., de Lima Morais, D. A., Chang, L., Barrette, M., Gauthier, C., Jacques, P. E., Li, S., and Xia, J.: MetaboAnalyst 5.0: narrowing the gap between raw spectra and functional insights, Nucleic Acids Res, 49, W388-W396, https://doi.org/10.1093/nar/gkab382, 2021.

Sá-Pessoa, J., Paiva, S., Ribas, D., Silva, I. J., Viegas, S. C., Arraiano, C. M., and Casal, M.: SATP (YaaH), a succinate–acetate transporter protein in Escherichia coli, Biochemical journal, 454, 585-595, https://doi.org/10.1042/BJ20130412, 2013.

Seemann, T.: Prokka: rapid prokaryotic genome annotation, Bioinformatics, 30, 2068-2069, https://doi.org/10.1093/bioinformatics/btu153, 2014.

Song, F. and Gao, Y.: Chemical characteristics of precipitation at metropolitan Newark in the US East Coast, Atmospheric Environment, 43, 4903-4913, https://doi.org/10.1016/j.atmosenv.2009.07.024, 2009.

Sun, X., Wang, Y., Li, H., Yang, X., Sun, L., Wang, X., Wang, T., and Wang, W.: Organic acids in cloud water and rainwater at a mountain site in acid rain areas of South China, Environ Sci Pollut Res Int, 23, 9529-9539, https://doi.org/10.1007/s11356-016-6038-1, 2016.

Sündermann, A., Eggers, L. F., and Schwudke, D.: Liquid Extraction: Bligh and Dyer, in: Encyclopedia of Lipidomics, 1-4, https://doi.org/10.1007/978-94-007-7864-1_88-1, 2016.

Tsai, Y. I. and Kuo, S.-C.: Contributions of low molecular weight carboxylic acids to aerosols and wet deposition in a natural subtropical broad-leaved forest environment, Atmospheric Environment, 81, 270-279, https://doi.org/10.1016/j.atmosenv.2013.08.061, 2013.

Vaitilingom, M., Deguillaume, L., Vinatier, V., Sancelme, M., Amato, P., Chaumerliac, N., and Delort, A. M.: Potential impact of microbial activity on the oxidant capacity and organic carbon budget in clouds, Proc Natl Acad Sci U S A, 110, 559-564, https://doi.org/10.1073/pnas.1205743110, 2013.

Vaïtilingom, M., Attard, E., Gaiani, N., Sancelme, M., Deguillaume, L., Flossmann, A. I., Amato, P., and Delort, A.-M.: Long-term features of cloud microbiology at the puy de Dôme (France), Atmospheric Environment, 56, 88-100,

https://doi.org/10.1016/j.atmosenv.2012.03.072, 2012.

Wang, Y., Sun, M., Li, P., Li, Y., Xue, L., and Wang, W.: Variation of low molecular weight organic acids in precipitation and cloudwater at high elevation in South China, Atmospheric environment, 45, 6518-6525, https://doi.org/10.1016/j.atmosenv.2011.08.064, 2011.

Wobrock, W., Schell, D., Maser, R., Jaeschke, W., Georgii, H.-W., Wieprecht, W., Arends, B., Mols, J., Kos, G., and Fuzzi, S.: The Kleiner Feldberg Cloud Experiment 1990. An overview, Journal of Atmospheric Chemistry, 19, 3-35, https://doi.org/10.1007/BF00696581, 1994.

Xu, G., Lee, X., and Lv, Y.: Urban and rural observations of carboxylic acids in rainwater in Southwest of China: the impact of urbanization, Journal of atmospheric chemistry, 62, 249-260, https://doi.org/10.1007/s10874-010-9151-4, 2009.

Zhang, Y., Lee, X., and Cao, F.: Chemical characteristics and sources of organic acids in precipitation at a semi-urban site in Southwest China, Atmospheric environment, 45, 413-419, https://doi.org/10.1016/j.atmosenv.2010.09.067, 2011.

Zhao, W., Wang, Z., Li, S., Li, L., Wei, L., Xie, Q., Yue, S., Li, T., Liang, Y., and Sun, Y.: Water-soluble low molecular weight organics in cloud water at Mt. Tai Mo Shan, Hong Kong, Science of the Total Environment, 697, 134095, https://doi.org/10.1016/j.scitotenv.2019.134095, 2019.